Optical Materials 122 (2021) 111742

Contents lists available at ScienceDirect

Optical Materials

journal homepage: www.elsevier.com/locate/optmat

Microstructural, linear and nonlinear optical study of spray pyrolysed nanostructured La–ZnO thin film: An effect of deposition temperature

A. Ayana [a], Parutagouda Shankaragouda Patil [b], Neelamma B. Gummagol [c], U.K. Goutam [d], Pankaj Sharma [e,f,**], B.V. Rajendra [a,*]

[a] Department of Physics, Manipal Institute of Technology, Manipal Academy of Higher Education, Manipal, 576104, India
[b] Department of Physics, B.L.D.E. Association's S.B. Arts and K.C.P. Science College, Vijayapura, 586103, Karnataka, India
[c] Department of Physics, K.L.E. Institute of Technology, Opposite Airport, Gokul, Hubballi, 580030, Karnataka, India
[d] Technical Physics Division, Bhabha Atomic Research Centre, Mumbai, 400085, India
[e] School of Materials Science and Engineering, The University of New South Wales (UNSW), Sydney, NSW, 2052, Australia
[f] ARC's Centre of Excellence in Future Low Energy Electronics Technologies (FLEET), UNSW Sydney, NSW, 2052, Australia

ARTICLE INFO

Keywords:
La doped ZnO films
Spray pyrolysis
Structural property
Nonlinear optical properties
Optical limiter

ABSTRACT

Transparent $Zn_{0.97}La_{0.03}O$ nanostructures were prepared at different temperatures (300 °C–500 °C) on borosilicate glass substrates using the chemical spray method. The present work focused on the dependence of the substrate temperature (T_s) on the different characteristics of the prepared films. In all the deposits, a polycrystalline structure of La^{3+} doped ZnO (LZO) film with a preferred orientation along the (101) plane was observed, and a larger crystalline size was noticed for films deposited at lower temperatures. The surface morphology changed from spherical to fibrous structure as a function of the temperature of the substrate. The chemical state and elemental compositions were confirmed by XPS analysis. The linear optical band gap and third-order nonlinear absorption coefficient of LZO films were observed to increase with an increase in substrate temperature. A maximum transmittance was observed for the sample prepared at 450 °C with the least optical limiting threshold value of 0.96 kJ/cm^2. The presence of various defects in the film was confirmed through photoluminescence emission, and red emission was noticed for samples prepared at 450 °C and 500 °C.

1. Introduction

Nonlinear optics (NLO) has been a rapidly expanding scientific field in recent decades due to vast optical applications, including optical signal processing, ultrafast switches, sensors, ultrashort pulsed lasers, laser amplifiers, and many others [1,2]. NLO is the study of the nonlinear interaction between light and matter that occurs when light-induced changes in the optical characteristics of the medium occur. Among the various NLO materials studied, semiconductors with wide bandgap, particularly Zinc Oxide (ZnO), exhibit appealing nonlinear optical properties, making them an interesting candidate for devices based on NLO [1,3]. Furthermore, due to its unique properties, such as the absence of a center of symmetry in the wurtzite structure and high electromechanical coupling, it is a good piezoelectric semiconductor material and has significant applications in mechanical actuators, chemical sensors, solar cells, and piezoelectric sensors [4–6]. ZnO thin films can be deposited using various methods like thermal evaporation [7], sputtering [8], sol-gel [9], pulsed laser deposition [10], molecular beam epitaxy [11], and chemical spray pyrolysis [12]. The chemical spraying method is a low-cost and simple technique that can be very beneficial for wide-area applications.

Intentional impurity addition to a ZnO nanostructure during its growth process causes significant changes in functional properties, including linear and nonlinear optical properties. Several studies were conducted on the NLO properties of ZnO using nanosecond lasers, including the effect of various dopants and film deposition temperature [13–17]. However, there is a very limited number of reports describing the NLO properties of rare-earth-doped ZnO samples. Among them, there are no reports available on the NLO properties of LZO thin film. La is one of the most reactive elements in the lanthanide group, and its wide bandgap makes it more suited for optical applications. We have already reported that a 3 at. % La-doped ZnO sample is better suited for optical

* Corresponding author.
** Corresponding author. School of Materials Science and Engineering, The University of New South Wales (UNSW), Sydney, NSW, 2052, Australia.
E-mail addresses: pankaj.sharma@unsw.edu.au (P. Sharma), bv.rajendra@manipal.edu (B.V. Rajendra).

https://doi.org/10.1016/j.optmat.2021.111742
Received 15 September 2021; Received in revised form 16 October 2021; Accepted 28 October 2021

liming applications in our previous paper of $Zn_{1-x}La_xO$ films [17]. As a follow-up, we investigated the influence of the temperature of the substrate on the 3 at. % La-doped ZnO samples for applications in optical limiting.

The current work reports the effect of temperature of the substrate on the different properties of the spray pyrolyzed $Zn_{0.97}La_{0.03}O$ thin films, such as microstructure, morphology, elemental composition, linear and nonlinear optical characteristics. A thorough study of the characteristics of deposit films helps to understand their relationship and their effects on optical limiting properties.

2. Experimental details

To prepare $Zn_{0.97}La_{0.03}O$ thin film, Zinc acetate ($Zn(CH_3COO)_2.2H_2O$) as the host-matrix, and Lanthanum chloride ($LaCl_3.7H_2O$) as dopant, of the required amount, were dissolved in double distilled water for getting total molar concentration of 0.05 M. The deposition temperatures were taken from 300 °C to 500 °C with a step difference of 50 °C, and the solution flow rate was kept at 2 ml/min onto the preheated substrate using compressed air with a pressure of 6 kg/cm^2. The distance between nozzle and substrate was fixed at 28 cm, and the film thickness 500–550 nm was maintained. After the deposition, samples were maintained at the same substrate temperature for 30 min to eliminate unreacted precursors from the samples.

The structural analysis was carried out at room temperature using Cu Kα (=1.5405 Å) monochromatic radiation with a step size of 0.1^0 using Rigaku-Miniflex 600, and the surface profilometer was used to measure the thickness of the film. The microstructures of the samples were recorded by SEM, and EDAX was used to identify the elemental composition. X-ray photoelectron spectroscopy (XPS) was performed to find out the chemical state and elemental composition using HAXPES beamline (PES-BL14) at Indus-synchrotron source having Si(111) based double crystal monochromator and Phoibos-225 hemispherical energy analyzer with X-ray energy of 4339eV for the samples [18]. Shimadzu-1800 UV-VIS spectrometer in the range from 350 to 800 nm at room temperature was used for measuring the optical response of the films, and the photoluminescence (PL) spectra were studied with Jasco FP-8300 fluorescence spectrometer. The third-order NLO studies have been done using Z-scan technique with a CW DSSP laser at 532 nm wavelength. The closed aperture (CA) and open aperture (OA) Z-scan experiments were conducted to investigate the intensity dependence of nonlinear refraction and nonlinear absorption of materials, respectively.

3. Results and discussions

3.1. Structural analysis

All deposits (Fig. 1) showed a polycrystalline nature with several diffraction peaks corresponding to (1 0 0), (0 0 2), (1 0 1), (1 0 2), (1 1 0), (1 0 3) and (112) plane of ZnO. The film exhibited a hexagonal wurtzite structure, with the highest intensity of diffraction peak corresponding to the (101) plane, implying that grains orient in a direction other than the c-axis, and similar results were observed in various literature [19,20]. Within the XRD detection limits, no phases related to La, e.g., La_2O_3, or other impurity phases, were detected in the La–ZnO thin films. This suggests that La^{3+} either enters the interstitial sites or replaces a few Zn^{2+} ions. The diffraction peak intensity of all the deposits decreased with increasing deposition temperature, with the maximum being at 300 °C. The average crystalline size, calculated using the Scherrer formula [17] for prominent (101) crystalline peaks, shows a reduction until 450 °C, and then it increases again. It is reasonable to assume that deposition temperature increase causes enhanced mobility of the adatoms. Consequently, the higher ionic radii doping element (La^{3+}) can easily occupy interstitial positions in the ZnO host matrix, causing lattice strain, which likely suppresses the growth of ZnO crystallites, and thus their size. Furthermore, the diffraction peaks move to

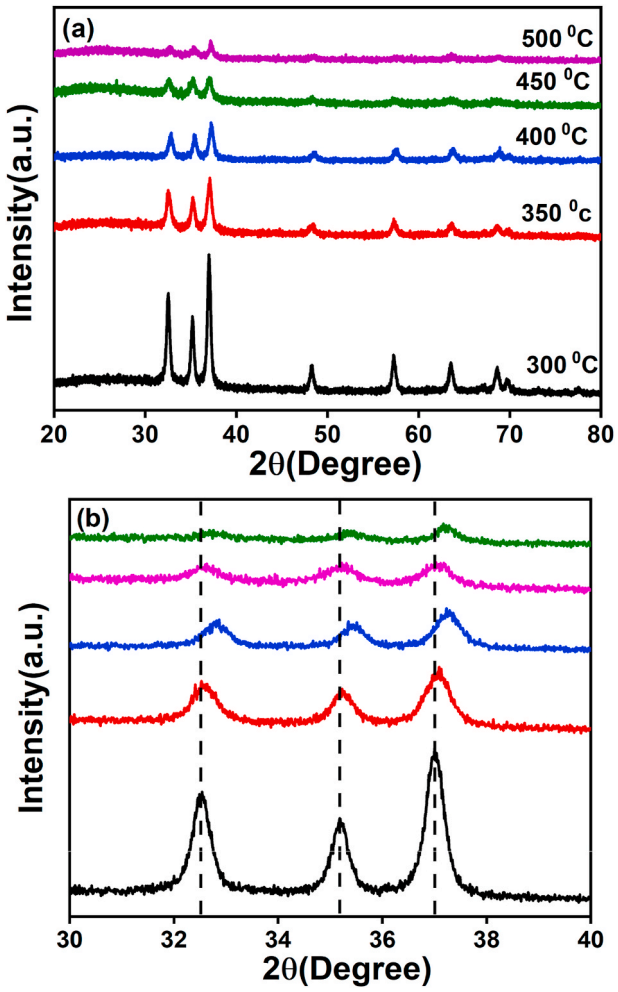

Fig. 1. XRD pattern of $Zn_{0.97}La_{0.03}O$ films (a) 20-80^0, and (b) 30-40^0 deposited at 300 ^{0}C-500 °C temperatures.

the higher angles until 400 °C, then back to the lower angles at 450 °C, followed by a reversal again at the highest deposition temperature. This is due to the changes in lattice parameter values (shown in Table 1), arising because the film growth temperature plays an important role in the nucleation and growth of crystallites.

Further, the lattice strain induced in the film can be determined by using the equation,

$$\varepsilon = \frac{\beta \cos\theta}{4} \quad (1)$$

According to Bragg's law, the spacing between the interatomic planes is,

$$n\lambda = 2d\sin\theta \quad (2)$$

The calculated inter-planar distance (d) is found to be higher for the sample prepared at 450 °C. The increase in d spacing is associated with the large ionic radii difference between La^{3+} and Zn^{2+} ions, resulting in the substitution of larger La^{3+} ions into the space of smaller Zn^{2+} ions sites. The change in lattice parameter values indicates that the introduction of dopant ions at different temperatures alters the structure of ZnO and the La ion disperses homogeneously in the ZnO matrix.

The dislocation density (δ) can be calculated from the crystalline size of the prepared nanostructure using the relation,

$$\delta = \frac{1}{D^2} \quad (3)$$

The determined dislocation density exhibited an increasing trend

Table 1
Crystalline size, inter-planar spacing, strain, dislocation density, and lattice parameter values of $Zn_{0.97}La_{0.03}O$ films deposited using 0.05 M concentration at different temperatures.

Samples No.	Temperature (°C)	Crystalline Size D (nm)		d (Å)	Strain × 10^{-3}	Dislocation density × 10^{15} [lines/m^2]	Lattice Parameters		
		Scherrer Formula	W–H Method				a (Å)	c (Å)	Cell volume (Å)
LZO-1	300	19.043	24.760	2.427	1.820	2.758	3.211	5.141	45.913
LZO-2	350	16.877	23.906	2.413	2.054	3.511	3.197	5.126	45.372
LZO-3	400	14.224	18.737	2.411	2.437	4.943	3.197	5.199	45.339
LZO-4	450	12.434	12.651	2.435	2.788	6.468	3.217	5.153	46.195
LZO-5	500	16.522	19.751	2.413	2.098	3.885	3.198	5.124	45.395

with an increase in substrate temperature and particle size. The estimated crystalline size of the sample was further confirmed using the Williamson-Hall method, and the relationship is given by,

$$\beta \cos\theta = \frac{k\lambda}{D} + 4\varepsilon \sin\theta \quad (4)$$

The calculated average crystalline size values from the W–H plot (Fig. 2) show a similar trend to those obtained using the Scherrer formula (Table 1).

3.2. Surface analysis

The morphological variation of $Zn_{0.97}La_{0.03}O$ films at different deposition temperatures is depicted in Fig. 3. The morphology of the sample obtained at 300 °C was spherical, with inter-granular porosity on the surface, and as the temperature increased, the morphology changed from spherical to a needle-like structure. An evolving fibrous structure was noticed as the temperature rises to 500 °C, comparable to the pure ZnO reported in our prior study [17]. The spherical structure at lower

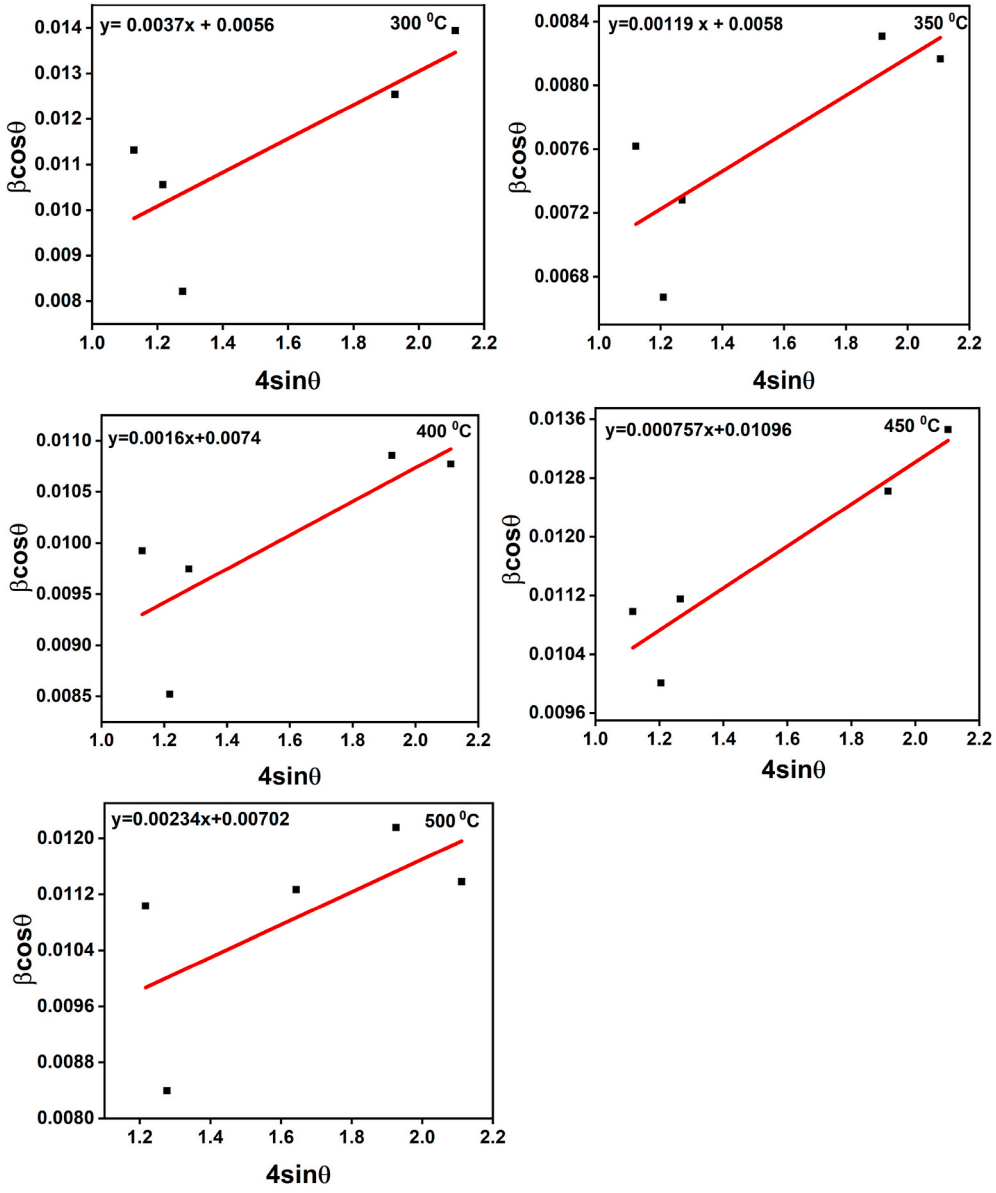

Fig. 2. W–H plot of $Zn_{0.97}La_{0.03}O$ film prepared at different temperatures.

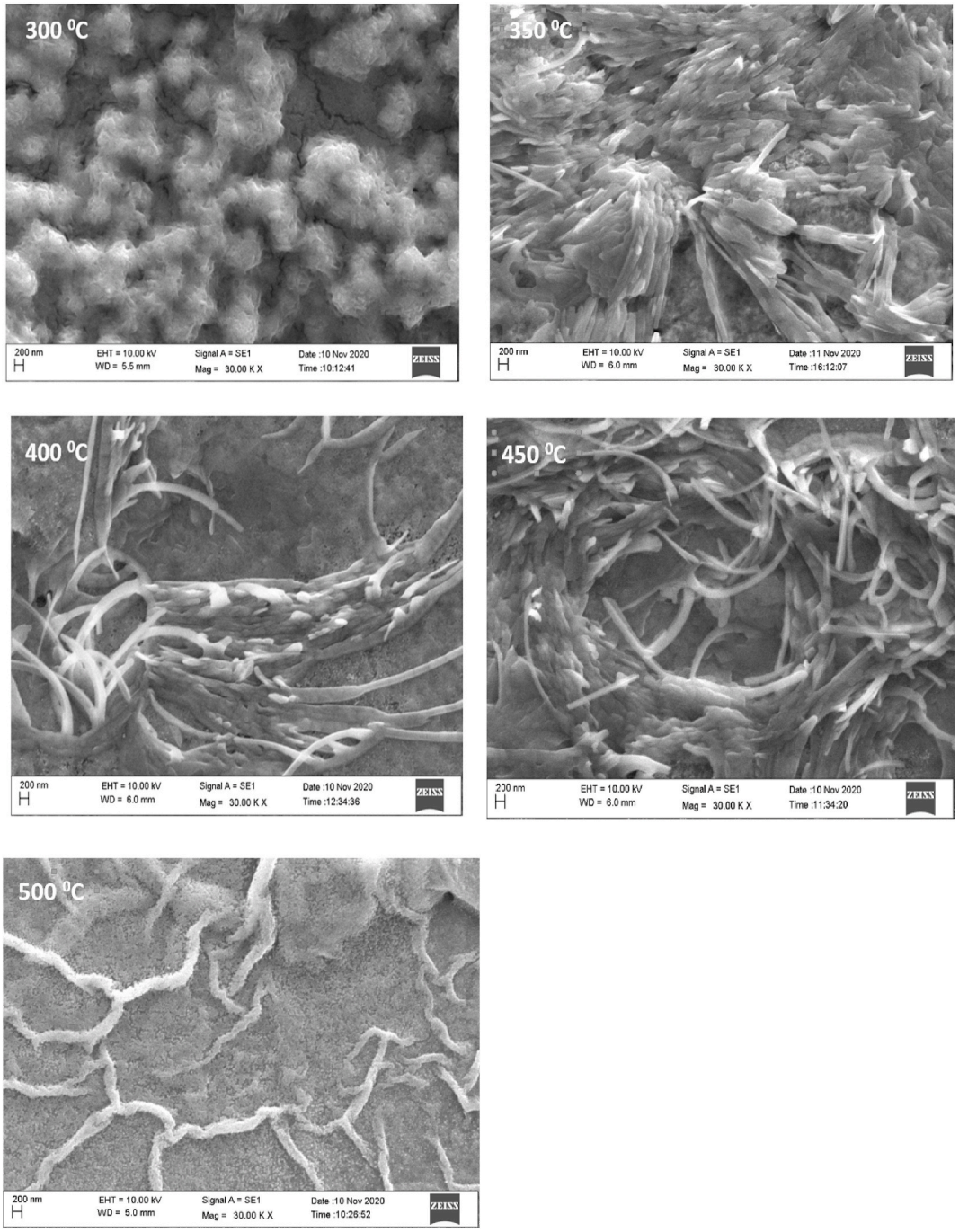

Fig. 3. SEM images of $Zn_{0.97}La_{0.03}O$ deposited at different temperatures.

temperatures may be owing to particle agglomeration caused by decreased mobility of atoms. A steady transition in morphology can be noticed with increasing temperature, such as needles emanating from these small granules. This is mostly owing to the improved migratory ability of atoms at higher substrate temperatures during the growth process. The increase in deposition temperature resulted in increased film stress. As a result, here, it can see the deterioration of nanostructure with the rise in the substrate temperature. This is consistent with our XRD studies. Jia et al. [21] noticed an average diameter of 15–25 nm wire-like structure for La-doped ZnO. In contrast, Ahmed et al. [22] reported a cracked surface for pure ZnO, which was modified to be more spherical in the presence of La prepared at 450 °C using the spray method. Similarly, Chandekar et al. [19] noticed a randomly aligned oval and spherical shape morphology of ZnO and as well as an agglomeration of fine nanoparticles owing to higher levels of defects with La concentration. Not only the temperature but the lattice strain created in the film also has a vital role in deciding the morphology of doped material as a result of higher ionic radii dopant. The obtained images implied that LZO films have a large surface area and hence can be considered as a suitable candidate for gas sensing applications.

3.3. Compositional analysis

The elemental mapping of EDAX spectra (Fig. 4) showed that Zinc, Oxygen, and Lanthanum were properly distributed in the deposits. The chemical constituents of the deposits were confirmed by analysis of EDAX spectra, which includes the requisite proportions of Zn, O, and La. The Silicon and Calcium peaks were neglected from the spectra as they

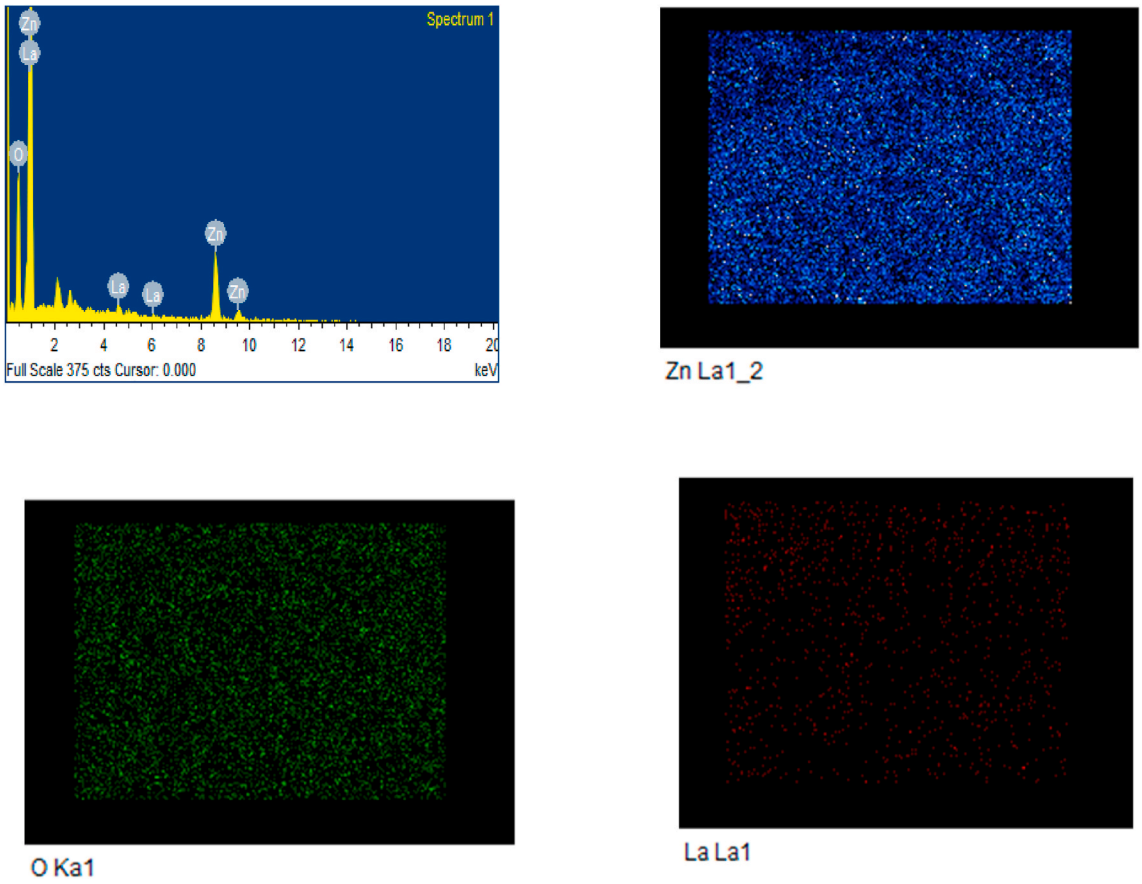

Fig. 4. Elemental morphology of Zn, O, and La with EDS spectra recorded for $Zn_{0.97}La_{0.03}O$ film deposited 400 °C.

were all caused by the substrate. The sample prepared at 450 °C showed a higher La content, indicating that dopant ions have been successfully incorporated. The observed and expected La content showed a slight variation in the elemental composition data given in Table 2.

3.4. XPS analysis

The chemical state and elemental composition of the samples prepared at 450 °C are further confirmed by XPS analysis. The observed peak at 284.54 eV represented the C 1s peak, and it is standardized as a reference. Fig. 5(a) shows the survey spectrum of $Zn_{0.97}La_{0.03}O$ film, which confirmed the presence of Zn, O, and La in the deposits. Due to strong spin-orbit coupling, the two peaks observed (Fig. 5(b)) at 1043.49 eV and 1020.36 eV are associated with $2p_{1/2}$ and $2p_{3/2}$, respectively. The main peaks of $Zn2p_{3/2}$ and $Zn2p_{1/2}$ are associated with Zn^{2+} in the wurtzite structure of ZnO. The observed difference in the binding energy value is 23.13 eV, which is within the standard reference value, confirming that the Zn element existed in the +2 oxidation state. Besides, compared to pure ZnO, a slight shift of the Zn spectrum of LZO nanostructure was observed. The primary cause of this shift might be owing to the presence of Zn–O–La bonding [23]. The deconvoluted asymmetric O 1s peak centered at three different binding energies is depicted in Fig. 5(c). The lower binding energy at 528.38ev is associated with oxygen present in the ZnO matrix. In ZnO nanostructure, each oxygen atom is surrounded by four Zinc atoms and conversely. Hence, this binding energy is due to the Zn–O bonds. The peak at 529.70 eV is related to O^{2-} ions that are in the oxygen-deficient region in the ZnO wurtzite structure. The peak at 531.16 eV of O 1s peak having higher binding energy could be attributed to the incorporation of oxygen in La–O–Zn. The deconvoluted doublet peak (Fig. 5 (d)) were found at 833.92 eV and 837.39 eV for La 3d5/2, and 850.78 eV and 853.99 eV for La 3d3/2 were in accordance with the standard binding energy of La. These values indicate that La existed in +3 oxidation state in the deposits. The peak with the highest energy is the contribution from the bonding between zinc and lanthanum, whereas the bonding between lanthanum oxide clusters contributes the lowest binding energy [24]. When compared to the conventional XPS energy peak position of La 3d in La_2O_3, the binding energy for the LZO nanostructure showed a slight blue shift. The shift may be owing to the change in length of the La–O bond in ZnO due to the proper incorporation of La ions in the ZnO lattice. Zhang et al. [25] explained it thus: the radius of La^{3+} (1.032 Å) ion is larger than that of Zn^{2+} (0.734 Å), the length of La–O bond should be reduced once the La^{3+} have been properly incorporated into the ZnO lattice and have replaced the Zn ion sites. Hence, the reduction in La–O bond length increases ion interaction, leading to a slight blue shift.

Table 2
Composition analysis of EDAX spectra of $Zn_{0.97}La_{0.03}O$ thin film.

Sample No	Temperature (°C)	Zn (at %)	O (at %)	La (at %)	x (La) "EDS" La content (at. %)
LZO-1	300	48.18	51.07	0.75	0.015
LZO-2	350	48.33	50.78	0.89	0.018
LZO-3	400	49.67	49.28	1.05	0.0207
LZO-4	450	50.36	48.38	1.26	0.027
LZO-5	500	49.96	48.87	1.17	0.023

3.5. Optical analysis

The transmittance spectra of $Zn_{0.97}La_{0.03}O$ film at different wavelengths are shown in Fig. 6. The deposited film had higher transparency (above 80%) in the visible region until 450 °C of substrate temperature,

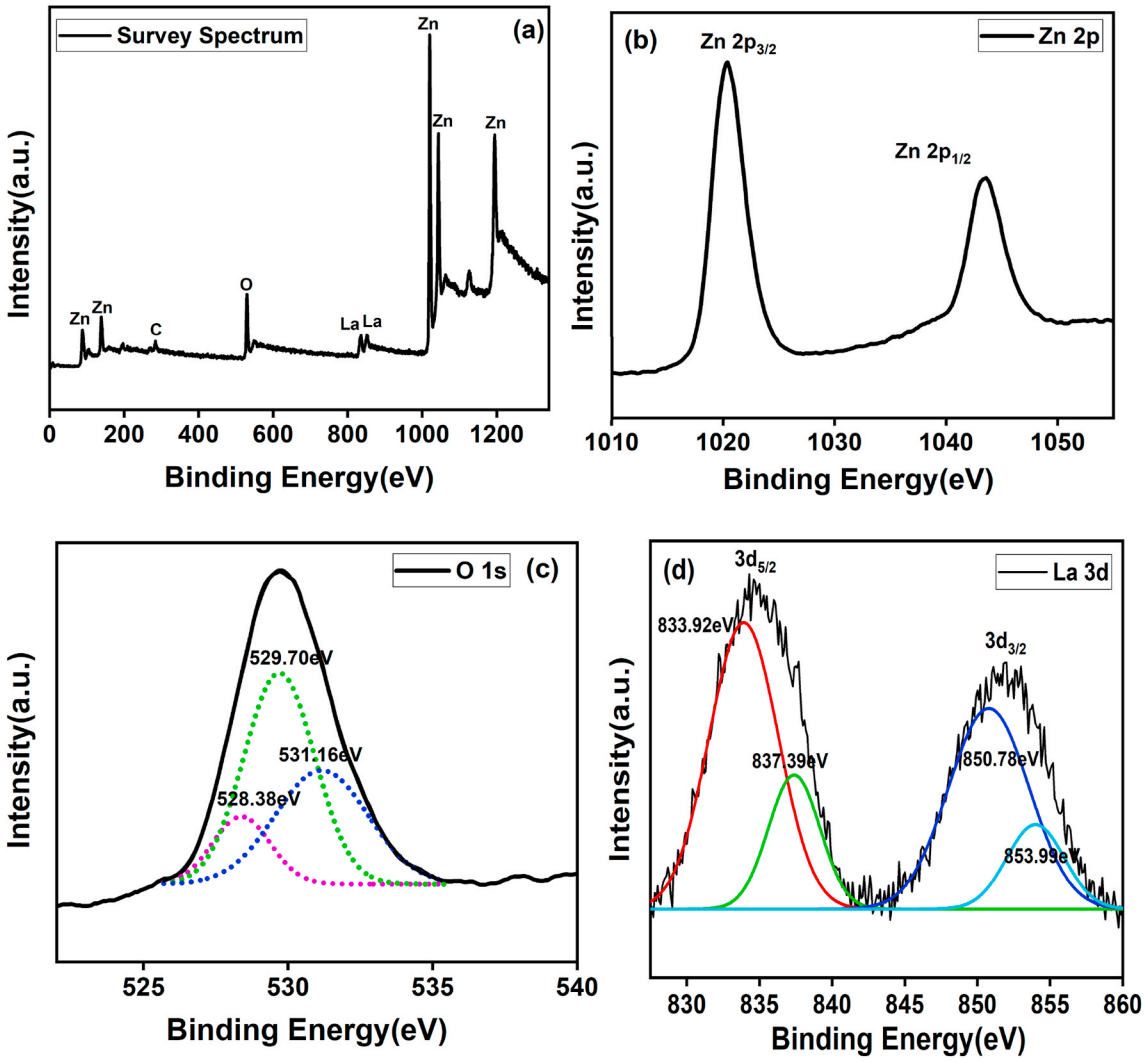

Fig. 5. XPS spectra of $Zn_{0.97}La_{0.03}O$ thin film (a) survey spectrum, (b) Zn 2p, (c) O 1s, and (d) La 3d.

after which it decreased slightly. The incomplete decomposition of the precursor at lower temperatures leads to lesser transparency of the deposits. The transmission is reduced when the film substrate temperature exceeds 450 °C. The increase in transparency is due to the structural change of deposits from granular to needle structure which is confirmed from the XRD and SEM study. The absorption edge had clearly shifted towards lower wavelengths which is quite apparent. similar behavior is observed by Rozati et al. [26] in In doped ZnO films at 450 °C. However, our results are contradictory to the already existing reports [19,20]. The bandgap energy is calculated from Tauc's plot relation, and it is given by,

$$(\alpha h\nu) = A\left(h\nu - E_g\right)^n \tag{5}$$

Where, $h\nu$ is the incident photon energy,α is the linear optical absorption coefficient, A is a constant, E_g is the optical bandgap energy, and n = ½ for direct allowed transition which characterizes the optical absorption process. A steady rise of the deposits energy bandgap values with temperature is believed to be caused by the Burstein-Moss (B-M) shift. The increase in temperature leads to an increase in carrier concentration. As the carrier concentration increases, light absorption by the carriers also increases, leading to a higher absorption coefficient [27]. The obtained results are well matching with our XRD results. Consistent with our results, Park et al. [28] noticed a gradual increase in the optical bandgap for Ga doped ZnO as the deposition temperature varied from 100 °C to 500 °C, whereas, Swapna et al. [29] found a reduction in bandgap with increasing temperature of the substrate of Mo: ZnO films deposited using the spray method on a glass substrate.

Refractive index (n) and extinction coefficient (k) values of prepared samples were estimated by the following equations,

$$n = \sqrt{H + \sqrt{\left(H^2 - S^2\right)}} \tag{6}$$

Where, $H = \frac{4s^2}{(s^2+1)T^2} - \frac{(s^2+1)}{2}$ (7)

$$k = \frac{\alpha\lambda}{4\pi} \tag{8}$$

Here, s is the refractive index of the substrate, and T is the transmittance of the deposits. The calculated n value of the film decreased with the increase of wavelength, which is associated with the dislocation density and strain induced in the film. The n value reduced from 3.56 to 2.02 at 450 nm when dislocation density increased from 2.758×10^{15} to 6.468×10^{15} lines/m^2 for film prepared from 300 °C to 500 °C, respectively. According to Ben et al. [30], when the strain field rises, the distribution of the refractive index around dislocations changes, resulting in scattering and interference as light passes through these refractive fields, causing the lowering of the refractive index of the film. The k values are also followed the same trend as the refractive index of the deposits and were found to be lower at 450 °C. These values are

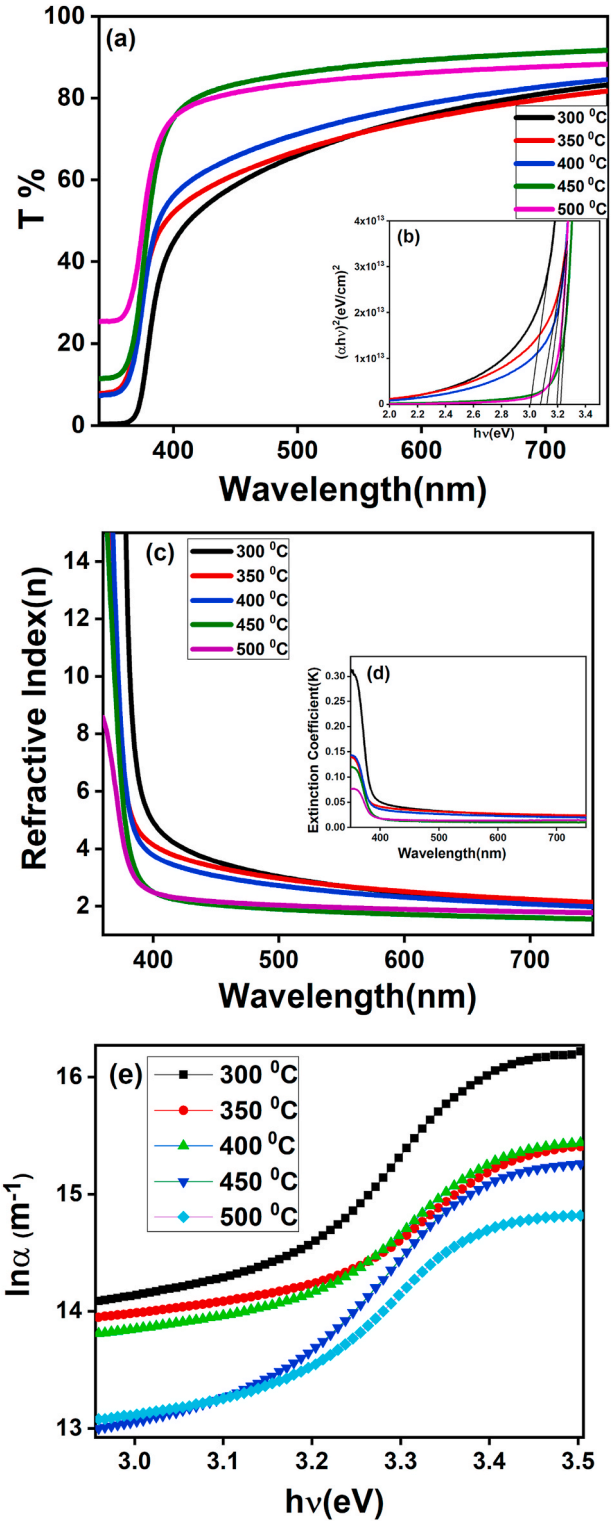

Fig. 6. Variation of transmission spectra (a) [(b) inset $(\alpha h\upsilon)^2$ Versus photon energy (hυ)], refractive index (c) [inset (d) extinction coefficient], Urbach energy (e) of $Zn_{0.97}La_{0.03}O$ film deposited at different temperatures.

consistent with already reported values of La-doped ZnO [31].

The disorders of the film were calculated by using Urbach energy (E_u), given by the equation,

$$\alpha = \alpha_0 \exp\left(h\nu/E_u\right) \quad (9)$$

where, α_0 is a constant. With increasing substrate temperature, the estimated Urbach energy values also increased. This energy is associated with microstructural lattice disorder, it is possible due to the inclusion of La ions can introduce new disorders and defects in LZO films with the increase in temperature (Table 3). The change of the energy bandgap and Urbach energy as a function of temperature on LZO films shows that the variation of E_g and E_u correlate well, and the E_u value is obtained more at 450 °C of substrate temperature. The estimated Eu value indicates that the disorderliness of the film increased with the temperature of the substrate, indicating that larger ionic radii La were incorporated into the ZnO lattice. In contrast, Tliba et al. [32] noticed a lesser Urbach energy of 52.02 meV for 3 wt% La-doped ZnO deposited at 375 °C using the spray method.

3.6. Photoluminescence analysis

The photoluminescence spectra of $Zn_{0.97}La_{0.03}O$ films deposited at various substrate temperatures are shown in Fig. 7. The spectra consist of emissions in both the ultraviolet and visible regions. The Near Band Edge (NBE) emission in the UV region is induced by free exciton recombination, whereas, the Deep Level Emission (DLE) in the visible region is believed to be caused by the electron-hole trapping at the induced defect and native centers in conduction and valence band, which releases photons of varying wavelengths. When the trivalent La ions replace the divalent Zn ions, the number of defects in the ZnO nanostructure such as zinc vacancies (V_{Zn}), oxygen interstitials (O_i), zinc interstitials (Zn_i), and oxygen vacancies (V_O) also increases. Fig. 6 revealed the reduction of the intensity of DLE emission peak, and a slight shift in peaks with the rise in temperature was also noticed, which might be due to the strain induced in the crystal lattice to accommodate larger La ions. Panatarani et al. [33] noticed a similar trend of 0.3 eV redshift in the peak of La-doped ZnO prepared using the spray technique. In contrast, Castaneda et al. [13] observed a slight blueshift when the substrate temperature of Indium-doped ZnO films increased from 385 °C to 445 °C using the same spray pyrolysis method.

The deconvoluted PL spectra of the deposits at various substrate temperatures are depicted in fig(6) (Table 4). The intensity of UV-PL in the deposits observed between 378-380 nm and 392–396 nm, which may be attributed to the density of free exciton, and these are closely associated to the crystallinity of the films. The emission peak between 420 and 424 nm may be due to the transition from Zn_i to VB, and the two blue emission peaks were found between 449 and 452 nm, and 466–469 nm may also be ascribed to the transition from extended Zn_i states to VB. Green luminescence emission between 528 and 533 nm is primarily due to oxygen vacancies or oxygen interstitials which create defect centers in the band, whereas singly ionized oxygen vacancies or other defects caused the yellow-orange emission between 560 and 576 nm [20,34]. Besides, a red emission was noticed for the samples prepared at 450 °C and 500 °C. The broad red emission peak implies that the associated energy levels are deep donor- and/or acceptor-center with strong electron-phonon interaction [35]. This result correlates well with our UV–Vis data.

In general, luminescence is directly related to film crystallinity since the density of defects in the film reduces as crystallinity improves [36]. The stable chemical state of La dopant in the host matrix does not

Table 3
Estimated optical bandgap and Urbach energy of $Zn_{0.97}La_{0.03}O$ deposited at different temperatures.

Sample No	Temperature (°C)	Band gap (eV)	Urbach Energy (meV)
LZO-1	300	3.004	98.237
LZO-2	350	3.078	99.754
LZO-3	400	3.121	100.396
LZO-4	450	3.217	101.385
LZO-5	500	3.199	99.543

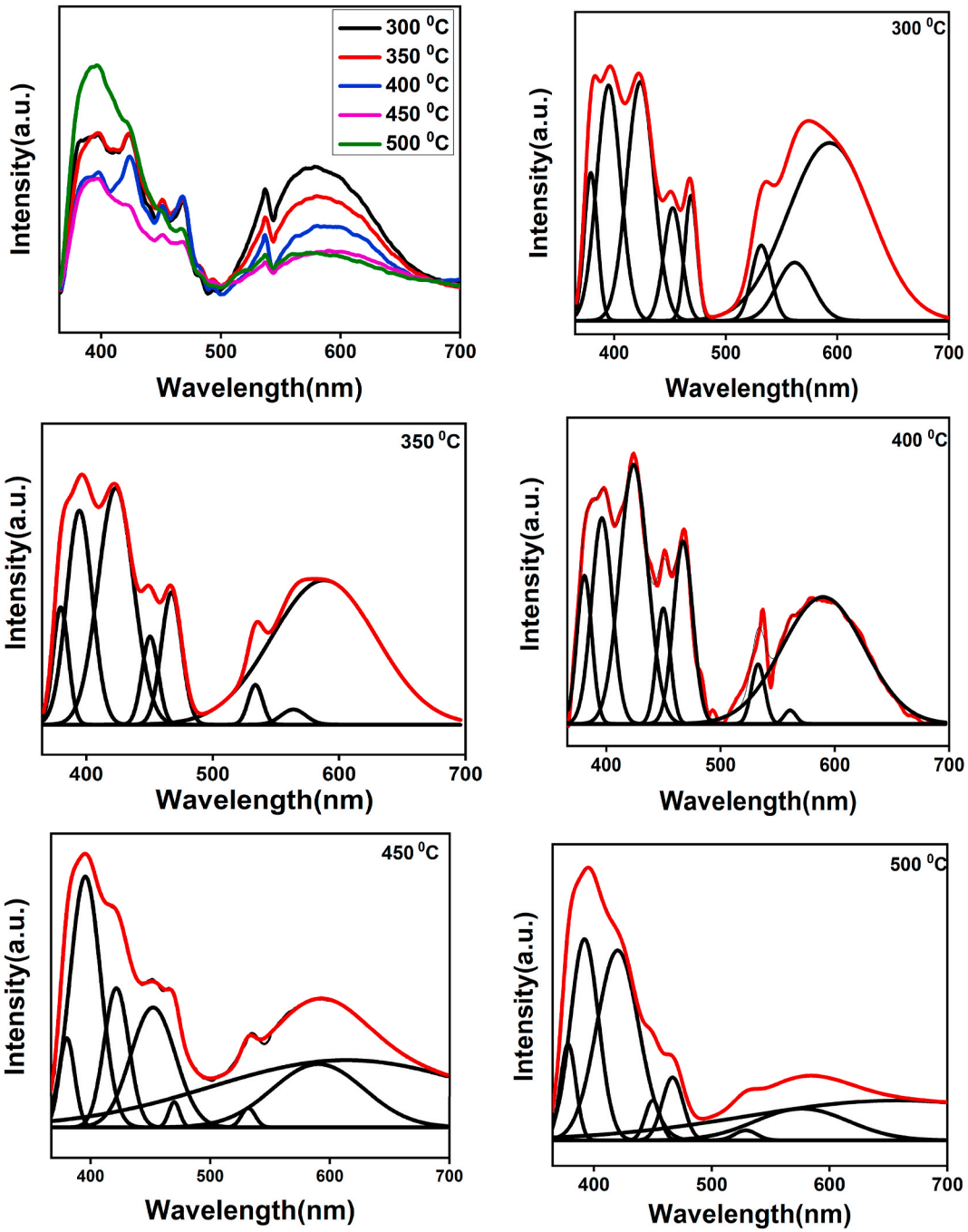

Fig. 7. Gaussian fit of photoluminescence spectra and deconvoluted photoluminescence spectra of $Zn_{0.97}La_{0.03}O$ film deposited at different temperatures.

Table 4
Deconvoluted La: ZnO peak in the UV-VIS region of $Zn_{0.97}La_{0.03}O$ deposited at different temperatures.

Sample No	Temperature (°C)	NBE		DLE						
LZO-1	300	379.102	395.055	423.465	452.520	468.863	531.904	561.850	593.114	
LZO-2	350	379.801	394.572	423.298	450.486	467.389	533.785	563.879	588.095	
LZO-3	400	380.947	396.237	424.050	449.960	467.276	532.887	560.904	589.763	
LZO-4	450	380.250	395.675	421.641	452.295	469.895	531.874		590.378	614.180
LZO-5	500	378.173	392.063	420.203	449.964	466.812	528.946	576.643		658.179

generate different PL spectra, as it is unable to capture electrons. However, it was noticed a red emission peak for the samples deposited at elevated temperatures. Jagtap et al. [37] observed a band at 509 nm due to yellow-green emission for La-doped ZnO, which they ascribed to deep level defect emission due to oxygen vacancies in ZnO nanostructure. Chandekar et al. [19] noticed a peak at 561 nm that corresponds to green emission as a result of the transition from the shallow donor level to the trapped holes at the oxygen vacancies. Hence, it is possible to

deduce that 3 at.% La doping into the ZnO host at various temperatures introduces new energy levels in the bandgap due to defect centers, which can improve its visible light response, which is advantageous for visible light-emitting LEDs, display, etc.

3.7. Nonlinear optical analysis

The open and closed apertures Z-scan curves for $Zn_{0.97}La_{0.03}O$ films are shown in Figs. 8 and 9, respectively. The shape of the OA curves indicates a reduction in normalized transmittance, suggesting that nonlinear absorption is owing to the reverse saturation absorption (RSA) process. The RSA process occurs for two reasons: (i) the absorption

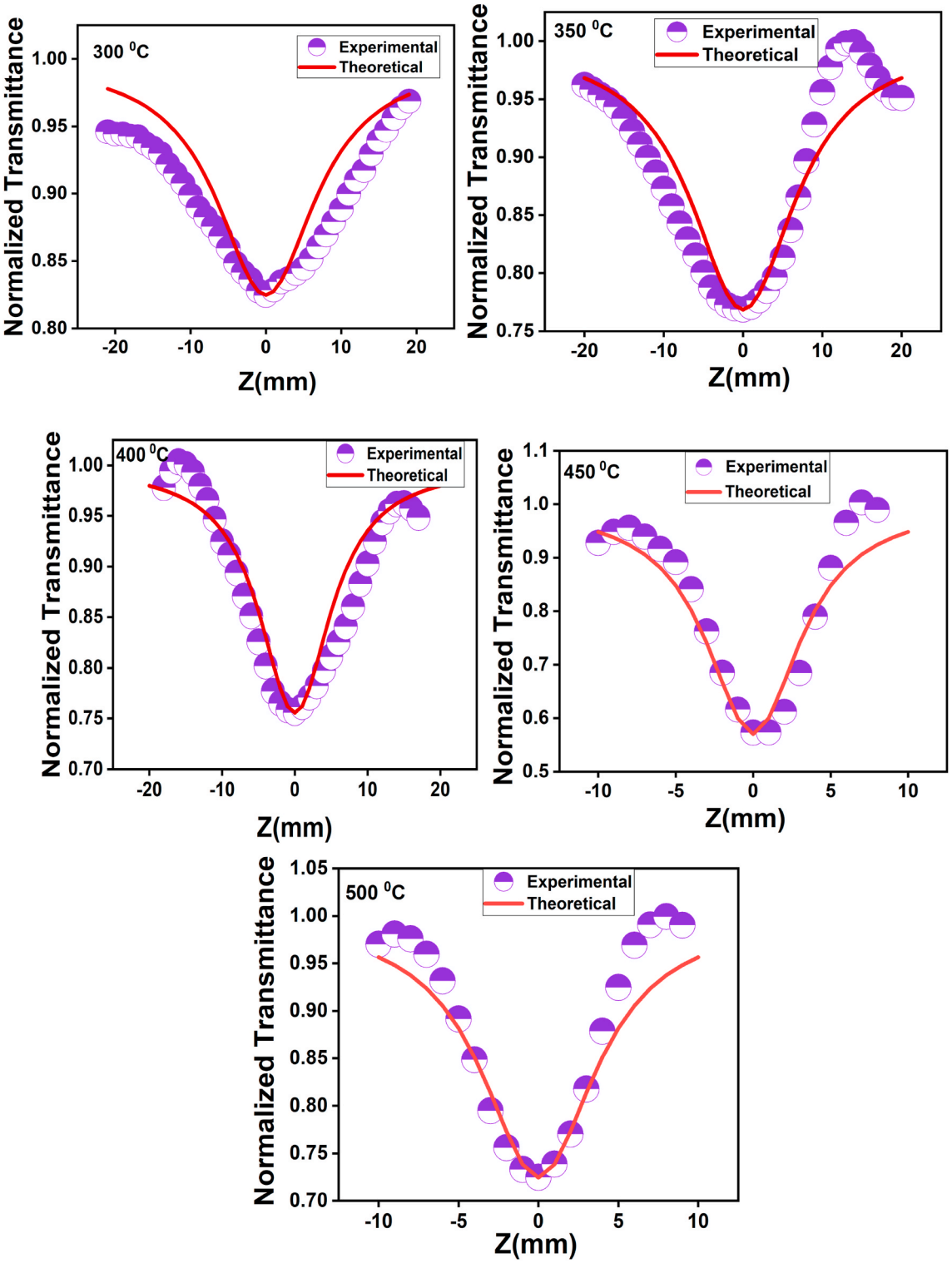

Fig. 8. Open aperture Z-scan curve of $Zn_{0.97}La_{0.03}O$ film deposited at different temperatures. Here the data points represent experimentally measured values, whereas the solid line represents a fit to experimental data.

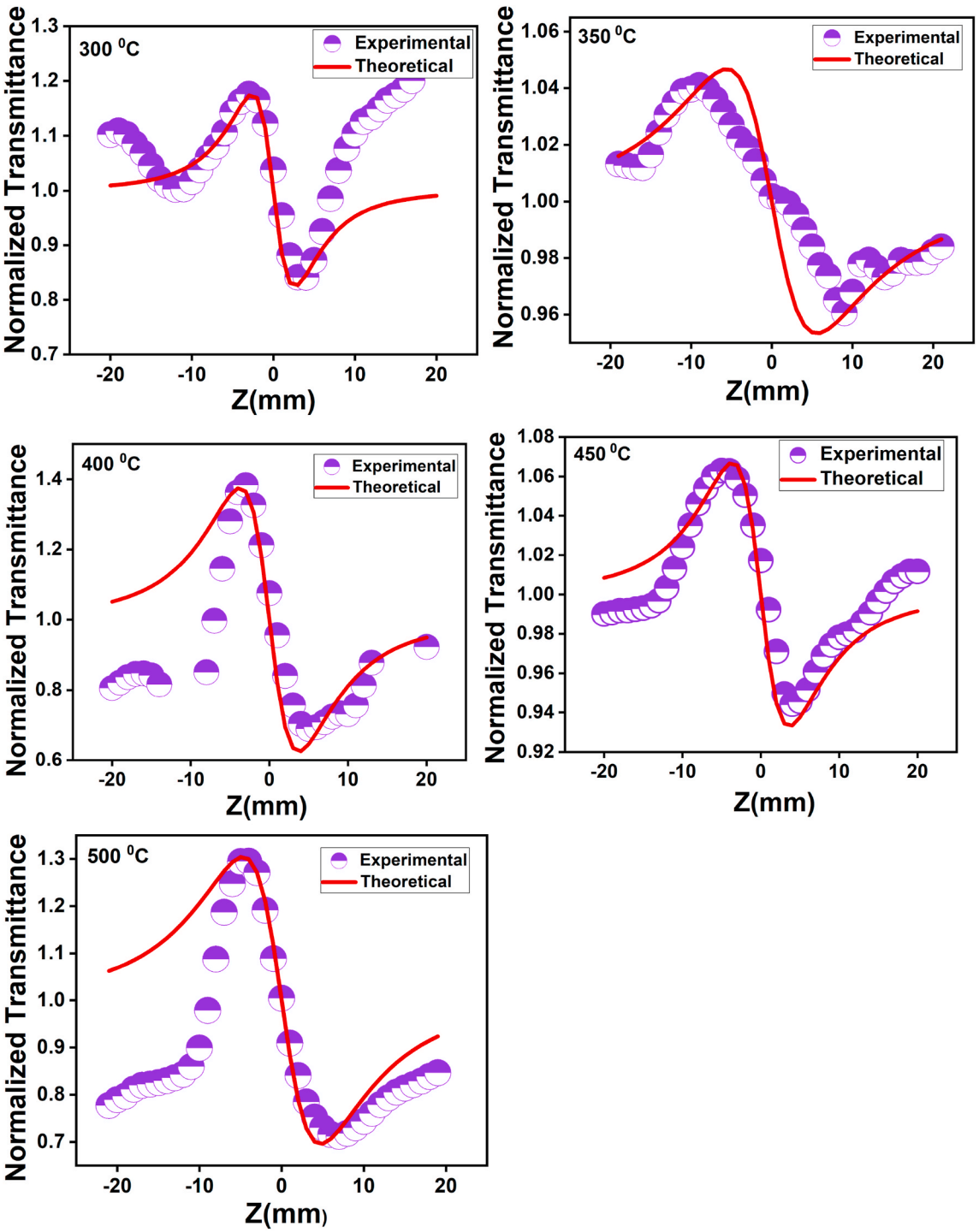

Fig. 9. Closed aperture Z-scan curve of $Zn_{0.97}La_{0.03}O$ film deposited at different temperatures. Here the data points represent experimentally measured values, whereas the solid line represents a fit to experimental data.

cross-section of the excited states must be higher than that of the ground states, and (ii) the molecules in both excited and ground states may absorb incident photons having the same wavelengths [38]. RSA process can also occur due to nonlinear processes such as two-photon absorption (TPA), excited-state absorption (ESA), free carrier absorption (FCA), nonlinear scattering, etc. [39]. In this case, the nanostructures are well suited by TPA, and it dominates only when the incident photon energy is less than bandgap (E_g) but larger than half of the bandgap ($E_g/2$) of the sample. The quantifiable energy bandgap values satisfied the following condition. Using open aperture data, the third-order nonlinear absorption coefficient (β_{eff}) can be calculated and is given by,

$$T(z) = 1 - \frac{\beta I_0 L_{eff}}{2\sqrt{2}\left(1 + \left(\frac{z}{z_o}\right)^2\right)} \tag{10}$$

Where effective sample thickness (L_{eff}) is,

$$L_{eff} = \left(1 - e^{-\alpha L}\right) \tag{11}$$

L is the thickness of the sample, and α is the linear absorption

coefficient. The reduction in transmittance was observed in OA curves with the increase in substrate temperature, which occurs most often when the ground state absorption cross-section is less than the excited state absorption cross-section. Hence, the determined absorption coefficient values increased with the rise in substrate temperature, and it is observed to be maximum for the sample prepared at 450 °C. Ramya et al. [40] reported the influences of reaction temperature on the NLO characteristics of ZnO nanoparticles, and they noticed a similar trend as ours.

The CA experiments were performed to estimate the sign and magnitude of the nonlinear refractive index n_2. The value of n_2 can be estimated using the relation,

$$T(z) = 1 - \frac{4x\Delta\varphi_0}{(x^2+1)(x^2+9)} \tag{12}$$

Where $\Delta\varphi_0$ is estimated by the proper fitting of the closed aperture curve with the above theoretical equation, and the value of n_2 is determined by using the relation $n_2 = \frac{\Delta\varphi}{kL_{eff}I_0}$. To explain the observed nonlinear refractions of semiconductor nanostructures, several processes such as nonlinear scattering, electronic polarization, free carrier refraction, and thermal effects are proposed [41]. The estimated refractive index is owing to cumulative thermal heating in the medium induced by the CW laser beam. From the CA curve, it was not noticed any sign reversal of the nonlinear refractive index, and it is well understood that all the samples exhibited a self-defocusing property with a peak followed by a valley owing to thermo-optic effects as a result of enhanced defect concentration. With CW laser, the evaluated nonlinear optical parameters are sum of both the electronic and thermal nonlinearity. Under the implemented scheme, therefore, it is not possible to differentiate between these two effects. According to Rahulan et al. [42], a small amount of energy is absorbed by the defect locations during laser irradiation. Defects can act as exiting electron trapping centers, favoring the suppression of photo-induced electron-hole pair recombination. This creates considerable local heating due to the thermal agitation of the particles and causes a change in refraction. A decreasing tendency of n_2 was observed with an increase in substrate temperature and found to be lesser for the sample prepared at 450 °C. The changes in the crystallite size and surface morphology are likely the same for the sample deposited at 350 °C and 500 °C, which could explain the difference in peak and valley behaviour when compared to other deposits. The obtained data matches with linear optical data, which shows highly transparent film was obtained at 450 °C.

Third-order nonlinear susceptibility is the sum of susceptibilities of real and imaginary parts, and it is directly related to β and n_2 values given by:

$$\chi^{(3)} = \chi_R^{(3)} + \chi_I^{(3)} \tag{13}$$

Where

$$\chi_I^{(3)}(esu) = \frac{10^{-2}\varepsilon_0 c^2 n_0^2 \lambda}{4\pi^2}\beta_{eff} \quad (\mathrm{cm/W}) \tag{14}$$

and,

$$\chi_R^{(3)}(esu) = \frac{10^{-4}\varepsilon_0 c^2 n_0^2 n_2}{\pi} \quad (\mathrm{cm^2/W}) \tag{15}$$

Where, n_0, ε_0, and c are the linear refractive index, the permittivity of free space, and velocity of light in free space, respectively, and here, the imaginary part (eq. (14)) is related to β_{eff}, and the real part (eq. (15))is related to the n_2. The estimated nonlinear parameters are summarized in Table 5. The total susceptibility value is found to be maximized for the sample prepared for 400 °C, and materials with high nonlinear optical susceptibilities are desirable for nonlinear photonic applications such as optical switching, pulse power shaping in optical parametric oscillators, and other nonlinear optical applications.

According to Bahedi et al. [14], the substrate temperature affects the surface roughness of the film, and the changes in the surface roughness value influence the value of $\chi^{(3)}$. In other words, when roughness diminishes, susceptibility increases. They investigated the in fluence of temperature of the substrate on the NLO characteristics of Al doped ZnO and found that the 5% doped sample at 450 °C had the best susceptibility value, $\chi^{(3)} = 20.49 \times 10^{-12}$ (esu). Sofiani et al. [43] concluded that $\chi^{(3)}$value is connected to the quality of the film. They noticed the highest $\chi^{(3)}$ value of 6.38×10^{-13} esu for 0.8 at. % Ce doped ZnO at high deposition temperature of 500 °C. According to Seo et al. [44], surface morphology can have a significant impact on third order nonlinear properties. In the present work, obtained $\chi^{(3)}$ value is in the range of 10^{-4} esu, and this result is better than previous reports on rare-earth doped ZnO.

3.8. Optical limiting

Optical limiters transmit low-intensity light and become opaque when the input intensity is high. High linear transmittance, low limiting threshold (LT), stability, and other requirements are needed for materials to become good optical limiters [40]. The primary application of optical limiting is to protect sensitive optical components from being damaged by the high-intensity input light. Fig. 10 depicts the optical limiting behavior of the sample, in which the normalized transmittance decreases when the laser intensity is increased, and it is obtained from the open aperture Z-scan curve. The intensity of transmitted light at different Z-positions calculated from the laser fluence equation is given by,

$$I_0 = \frac{2P}{\pi\omega_z^2} \tag{16}$$

Where,

$$w_z = w_0\sqrt{1 + \left(\frac{z}{z_0}\right)^2} \tag{17}$$

The optical limiting characteristics observed in LZO nanostructured materials are owing to the two-photon-assisted RSA mechanism. The limiting threshold is observed to drop as the substrate temperature rises, showing improved optical limiting behavior (Table 5). The maximum and minimum LT values were obtained for the sample prepared at 450 °C, and 300 °C are 0.96 kJ/cm^2 and 2.78 kJ/cm^2, respectively. According to Ramya et al. [40], the particle size has an important effect on the optical limiting performance of nanostructures, and they reported an improvement in optical limiting performance as particle size increased, which contradicts our results. Compared to values from

Table 5
Third order nonlinear optical parameters of $Zn_{0.97}La_{0.03}O$ film deposited at different temperatures obtained from CW laser mode.

Sample No	Temperature (°C)	β_{eff} (× 10^{-1}) (cm/W)	$\chi_I^{(3)}$ (× 10^{-5}) (esu)	$\chi_R^{(3)}$(× 10^{-4}) (esu)	$\chi^{(3)}$ (× 10^{-4}) (esu)	n_2 (× 10^{-5}) (cm^2/W)	LT (kJ/cm^2)
LZO-1	300	6.80	57.5	20.12	20.93	−1.01	2.78
LZO-2	350	9.00	75.1	21.65	22.91	−1.09	1.51
LZO-3	400	9.24	64.9	34.71	35.31	−2.09	1.35
LZO-4	450	15.0	53.7	2.92	6.11	−0.34	0.96
LZO-5	500	9.75	40.9	15.76	16.28	−1.59	1.33

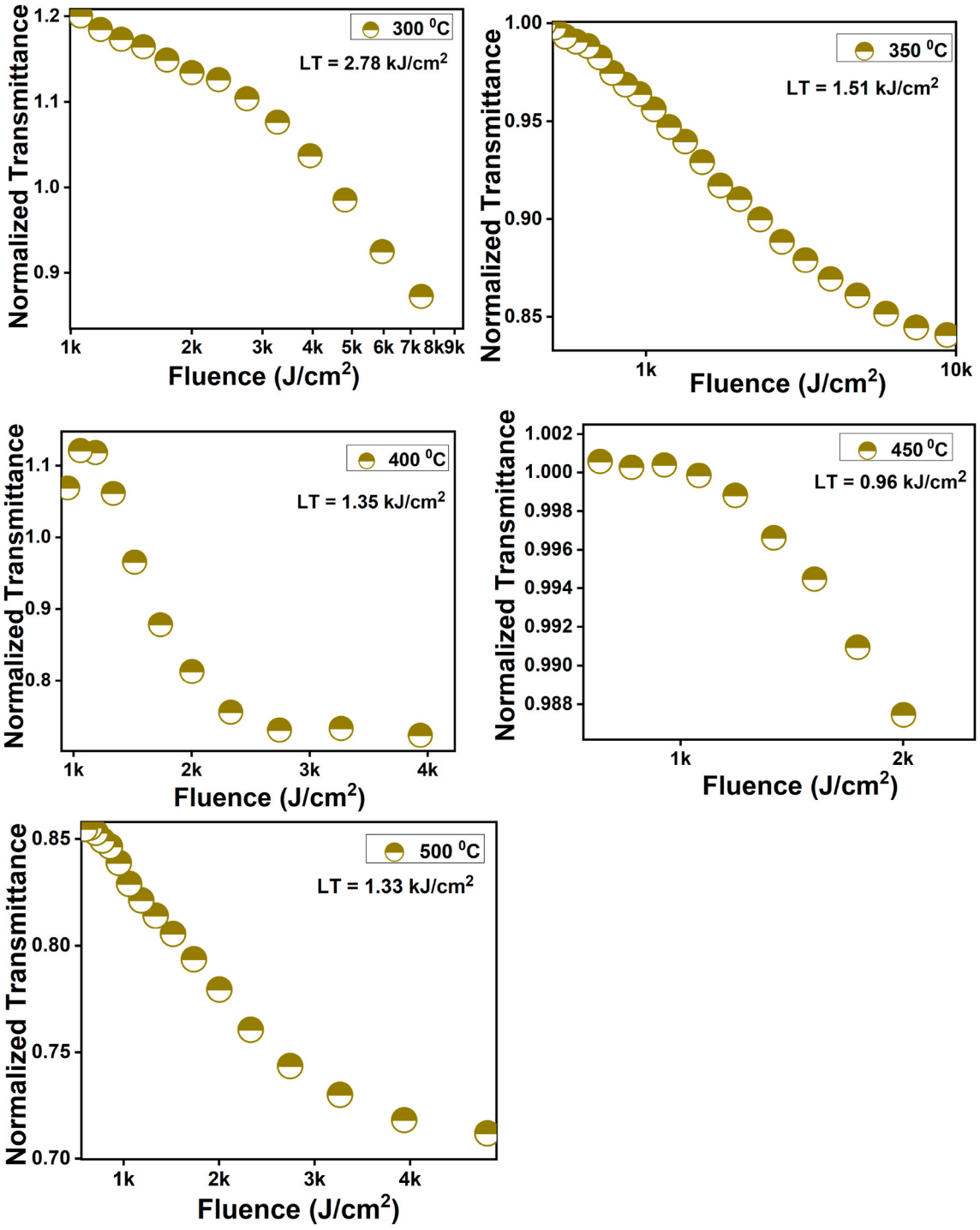

Fig. 10. Optical power limiting response of $Zn_{0.97}La_{0.03}O$ film deposited at different temperatures. It is estimated by fitting the experimental data from the z-scan measurements (shown in Figs. 8–9) using theoretical equations.

previous literature on metal-doped ZnO [39,45], our $Zn_{0.97}La_{0.03}O$ film prepared at different temperatures has the best optical limiting properties, among which, the sample deposited at 450 °C showed good optical limiting at high laser fluences and are suitable for shielding sensor devices [46].

4. Conclusions

The dependence of deposition temperature on different characteristics of $Zn_{0.97}La_{0.03}O$ nanostructured film prepared using the chemical spray pyrolysis method was investigated in depth. The deposits showed a hexagonal wurtzite structure with polycrystalline nature having a prominent (101) plane. The reduction in crystalline size and change in lattice parameters values confirmed the incorporation of La^{3+} into ZnO lattice with an increase in temperature. Morphological studies showed a change in surface morphology from spherical to fibrous with an increase in temperature. The elemental compositions and chemical state were confirmed by XPS analysis. The estimated optical bandgap value increased due to Burstein- Moss shift. The photoluminescence study showed the presence of defects and red emission for the samples

prepared at 450 °C and 500 °C. Enhancement of β_{eff} values were noticed with the increase in the deposition temperature of the samples. The film deposited at 450 °C showed a least optical limiting threshold value of 0.96 kJ/cm^2. Hence, the 3 at % La-doped ZnO film deposited at 450 °C displays the best optical limiting threshold value and can be a promising option for future photonic device applications.

CRediT author contribution statement

A. Ayana: is presently working , research scholar at the Department of Physics, Manipal Institute of Technology, MAHE, Manipal, India. She played role in data curation, Formal analysis, Investigation, and writing - original draft. **Parutagouda Shankaragouda Patil:** is a Assistant Professor at the Department of Physics in B.L.D.E.Association's S.B.Arts and K.C.P.Science College, Vijapura, Karnataka India. He played role in supervision and validation. **Neelamma B. Gummagol:** is a research scholar at the Department of Physics, KLEIT, Hubballi. She played role in data curation, Formal analysis, and Investigation. **U.K. Goutam:** is from Technical Physics Division, Bhabha Atomic Research Centre, Mumbai-India. He played role in data curation and formal analysis of the composition of the samples,. **Pankaj Sharma:** is a Lecturer at the School of Material Science and Engineering, The University of New South Wales (UNSW), Sydney, Australia. He played role in funding acquisition, Supervision, and validation. **B.V. Rajendra:** is a Associate Professor (Senior Scale) at the Department of Physics, Manipal Institute of Technology, MAHE, Manipal-India. He played role in funding acquisition, Resources, Software, Supervision, Validation, and writing - review and editing.

Declaration of competing interest

The authors declare that they have no known competing financial interests or personal relationships that could have appeared to influence the work reported in this paper.

Acknowledgment

The authors are grateful to acknowledge the financial support of UNSW-MAHE collaboration seed grant (RG194284-D). Ayana A would like to thank the Manipal Academy of Higher Education (MAHE) for giving a research fellowship. Authors express their gratitude to UGC-DAE-CSR consortium, Mumbai, for financial support [UDCSR/MUM/AO/CRS-M-315/2020/813]. Author thankful to RRCAT Indore for providing XPS measurements. The authors thank Dr. Sudha D Kamath for providing the photoluminescence facilities. Dr. P. S. Patil is grateful to Science and Engineering Research Board (SERB), Government of India, for the core research grant **(EMR/2017/003632)**.

References

[1] L. Irimpan, D. Ambika, V. Kumar, V.P.N. Nampoori, P. Radhakrishnan, Effect of annealing on the spectral and nonlinear optical characteristics of thin films of nano-ZnO Effect of annealing on the spectral and nonlinear optical characteristics of thin films of nano-ZnO 2008 (2012), 033118.

[2] E. Manikandan, V. Murugan, G. Kavitha, P. Babu, M. Maaza, "Nano fl ower rod wire-like structures of dual metal (Al and Cr) doped ZnO thin fi lms : structural , optical and electronic properties, Mater. Lett. 131 (2014) 225–228.

[3] C. Amirthavalli, A. Manikandan, A.A.M. Prince, E ff ect of zinc precursor ratio on morphology and luminescent properties of ZnO nanoparticles synthesized in CTAB medium, Ceram. Int. 44 (13) (2018) 15290–15297.

[4] E. Manikandan, M.K. Moodley, S.S. Ray, B.K. Panigrahi, R. Krishnan, N. Padhy, K. G.M. Nair, A.K. Tyagi, J. Kennedy, F. Fang, J. Futter, J. Leveneur, P.P. Murmu, G. N. Panin, T.W. Kang, E. Manikandan, Zinc Oxide Epitaxial Thin Film Deposited over Carbon on Various Substrate by Pulsed Laser Deposition Technique, 2010, pp. 5602–5611.

[5] S. Goel, N. Sinha, H. Yadav, J. Abhilash, B. Kumar, "Author ' s accepted manuscript, " *Phys. E Low-dimensional Syst. Nanostructures*, 2017.

[6] J. Kennedy, F. Fang, J. Futter, J. Leveneur, P.P. Murmu, G.N. Panin, T.W. Kang, E. Manikandan, Diamond & Related Materials Synthesis and enhanced fi eld emission of zinc oxide incorporated carbon nanotubes, Diam. Relat. Mater. 71 (2017) 79–84.

[7] A. Umar, R.I. Badran, A. Al-Hajry, S. Al-Heniti, Fabrication and characterization of n-Zno hexagonal nanorods/p-Si heterojunction diodes: temperature-dependant electrical characteristics, J. Nanosci. Nanotechnol. 15 (7) (2015) 4969–4975.

[8] B. Lin, Z. Fu, Y. Jia, Green luminescent center in undoped zinc oxide films deposited on silicon substrates, Appl. Phys. Lett. 79 (7) (2001) 943–945.

[9] S. Chauhan, M. Kumar, C. Anand, V. Dillu, R. Mazumdar, S.C. Katyal, Antibacterial activity and ferroelectric properties of Nd3+ doped ZnO nanostructured materials, AIP Conf. Proc. (2009) 1–5, 2018.

[10] E. Manikandan, G. Kavitha, J. Kennedy, Epitaxial zinc oxide , graphene oxide composite thin- fi lms by laser technique for micro-Raman and enhanced fi eld emission study, Ceram. Int. 40 (10) (2014) 16065–16070.

[11] Y.I. Alivov, Ü. Özgür, S. Doğan, D. Johnstone, V. Avrutin, N. Onojima, C. Liu, J. Xie, Q. Fan, H. Morkoç, Photoresponse of n-ZnO/p-SiC heterojunction diodes grown by plasma-assisted molecular-beam epitaxy, Appl. Phys. Lett. 86 (24) (2005) 1–3.

[12] Y. Bouznit, Y. Beggah, F. Ynineb, Sprayed lanthanum doped zinc oxide thin films, Appl. Surf. Sci. 258 (7) (2012) 2967–2971.

[13] L. Castañeda, D.R. Acosta, A. Maldonado, Structural , morphological , optical , and nonlinear optical properties of fluorine-doped zinc oxide thin films deposited on glass substrates by the chemical spray technique 1981 (8) (2006) 1971–1981.

[14] K. Bahedi, M. Addou, M. El Jouad, S. Bayoud, Z. Sofiani, Effects of deposition temperature on the surface roughness and the nonlinear optical susceptibility of sprayed deposited ZnO:Zr thin films, Appl. Surf. Sci. 255 (22) (2009) 9054–9057.

[15] A. Antony, S. Pramodini, P. Poornesh, I. V Kityk, A.O. Fedorchuk, In fl uence of electron beam irradiation on nonlinear optical properties of Al doped ZnO thin fi lms for optoelectronic device applications in the cw laser regime, Opt. Mater. 62 (2016) 64–71.

[16] M. Rajini, M. Karunakaran, K. Kasirajan, V. Annalakshmi, S. Rajasekar, Effect of substrate temperature on Mn doped CdO thin films prepared by perfume atomizer spray pyrolysis method 7 (3) (2019) 137–142.

[17] A. Ayana, N.B. Gummagol, P. Shankaragouda, P. Sharma, B. V Rajendra, Materials Science in Semiconductor Processing Enhancement of optical limiting performance in nanocrystalline La 3 + doped ZnO film, Mater. Sci. Semicond. Process. 133 (May) (2021) 105931.

[18] U.K. Goutam, R.K. Sharma, J. Singh, K. Dutta, U.S. Sule, S.C. Gadkari, HAXPES beamline PES-BL14 at the Indus-2 synchrotron radiation source, J. Synchrotron Radiat. 25 (5) (2018) 1541–1547.

[19] K.V. Chandekar, M. Shkir, A. Khan, B.M. Al-Shehri, M.S. Hamdy, S. AlFaify, M. A. El-Toni, A. Aldalbahi, A.A. Ansari, H. Ghaithan, A facile one-pot flash combustion synthesis of La@ZnO nanoparticles and their characterizations for optoelectronic and photocatalysis applications, J. Photochem. Photobiol. Chem. 395 (2020) 112465.

[20] A. Manikandan, E. Manikandan, B. Meenatchi, S. Vadivel, S.K. Jaganathan, Rare earth element (REE) lanthanum doped zinc oxide (La: ZnO) nanomaterials: synthesis structural optical and antibacterial studies, " *J. Alloys Compd.*, 2017.

[21] T. Jia, W. Wang, F. Long, Z. Fu, H. Wang, Q. Zhang, Fabrication , characterization and photocatalytic activity of La-doped ZnO nanowires 484 (2009) 410–415.

[22] M.M.A. Ahmed, W.Z. Tawfik, M.A.K. Elfayoumi, M. Abdel-Hafiez, S.I. El-Dek, Tailoring the optical and physical properties of La doped ZnO nanostructured thin films, J. Alloys Compd. 791 (2019) 586–592.

[23] P. Cao, D.X. Zhao, J.Y. Zhang, D.Z. Shen, Y.M. Lu, B. Yao, B.H. Li, Y. Bai, X.W. Fan, Optical and electrical properties of p-type ZnO fabricated by NH 3 plasma post-treated ZnO thin films, Appl. Surf. Sci. 254 (9) (2008) 2900–2904.

[24] S. Anandan, A. Vinu, K.S. Lovely, N. Gokulakrishnan, P. Srinivasu, T. Mori, V. Murugesan, V. Sivamurugan, K. Ariga, Photocatalytic activity of La-doped ZnO for the degradation of monocrotophos in aqueous suspension, J. Mol. Catal. Chem. 266 (1–2) (2007) 149–157.

[25] H.D. Zhang, M. Yu, J.C. Zhang, C.H. Sheng, X. Yan, W.P. Han, Y.C. Liu, S. Chen, G. Z. Shen, Y.Z. Long, Fabrication and photoelectric properties of La-doped p-type ZnO nanofibers and crossed p-n homojunctions by electrospinning, Nanoscale 7 (23) (2015) 10513–10518.

[26] S.M. Rozati, F. Zarenejad, N. Memarian, Study on physical properties of indium-doped zinc oxide deposited by spray pyrolysis technique, Thin Solid Films 520 (4) (2011) 1259–1262.

[27] S. Joishy, B.V. Rajendra, Effect of substrate temperature and molarity on optical and electrical properties of mixed structured Zn0.80Cd0.20O thin films, J. Electron. Mater. 47 (11) (2018) 6681–6690.

[28] S.M. Park, T. Ikegami, K. Ebihara, Effects of substrate temperature on the properties of Ga-doped ZnO by pulsed laser deposition, Thin Solid Films 513 (1–2) (2006) 90–94.

[29] R. Swapna, M.C. Santhosh Kumar, The role of substrate temperature on the properties of nanocrystalline Mo doped ZnO thin films by spray pyrolysis, Ceram. Int. 38 (5) (2012) 3875–3883.

[30] J. Ben, X. Sun, Y. Jia, K. Jiang, Z. Shi, Y. Wu, C. Kai, Y. Wang, X. Luo, Z.C. Feng, D. Li, Influence of dislocations on the refractive index of AlN by nanoscale strain field, *Nanoscale Res. Lett.* 14 (2019).

[31] D. Ali, M.Z. Butt, I. Muneer, M.A. Farrukh, M. Aftab, M. Saleem, F. Bashir, A. U. Khan, Synthesis and characterization of sol-gel derived La and Sm doped ZnO thin films: a solar light photo catalyst for methylene blue, in: Thin Solid Films, vol. 679, July 2018, pp. 86–98, 2019.

[32] M.T. Tliba, A. Benhaoua, R. Gheriani, B. Benhaoua, A. Rahal, C. Boukaous, A. Tliba, La-doped zno thin films prepared by spray pyrolysis withmoving nozzle: study of physical properties and adsorption ability of the copper, Dig. J. Nanomater. Biostructures 13 (4) (2018) 991–1002.

[33] C. Panatarani, F. Faizal, F.F. Florena, D. Jumhur, I. Made Joni, The effects of divalent and trivalent dopants on the luminescence properties of ZnO fine particle with oxygen vacancies, Adv. Powder Technol. 31 (7) (2020) 2605–2612.
[34] S. Vempati, J. Mitra, P. Dawson, One-step synthesis of ZnO nanosheets: a blue-white fluorophore, Nanoscale Res. Lett. 7 (2012) 1–10.
[35] V. Gokulakrishnan, S. Parthiban, K. Jeganathan, K. Ramamurthi, Applied Surface Science Investigation on the effect of Zr doping in ZnO thin films by spray pyrolysis, Appl. Surf. Sci. 257 (21) (2011) 9068–9072.
[36] X.Y. Li, H.J. Li, Z.J. Wang, H. Xia, Z.Y. Xiong, J.X. Wang, B.C. Yang, Effect of substrate temperature on the structural and optical properties of ZnO and Al-doped ZnO thin films prepared by dc magnetron sputtering, Opt Commun. 282 (2) (2009) 247–252.
[37] R.M. Jagtap, D.R. Kshirsagar, V.H. Khire, S.K. Pardeshi, Facile fabrication of porous La doped ZnO granular nanocrystallites and their catalytic evaluation towards thermal decomposition of ammonium perchlorate, J. Solid State Chem. 276 (April) (2019) 194–204.
[38] M. Abd-lefdil, A. Douayar, A. Belayachi, A.H. Reshak, A.O. Fedorchuk, S. Pramodini, Third harmonic generation process in Al doped ZnO thin films, J. Alloys Compd. 584 (2014) 7–12.
[39] V. Kumari, V. Kumar, B.P. Malik, R.M. Mehra, D. Mohan, Nonlinear optical properties of erbium doped zinc oxide (EZO) thin films, Opt Commun. 285 (8) (2012) 2182–2188.
[40] M. Ramya, T.K. Nideep, K.R. Vijesh, V.P.N. Nampoori, M. Kailasnath, Synthesis of stable ZnO nanocolloids with enhanced optical limiting properties via simple solution method, Opt. Mater. 81 (May) (2018) 30–36.
[41] U. Vinoditha, B.K. Sarojini, K.M. Sandeep, B. Narayana, S.R. Maidur, P.S. Patil, K. M. Balakrishna, Defects-induced nonlinear saturable absorption mechanism in europium-doped ZnO nanoparticles synthesized by facile hydrothermal method, Appl. Phys. Mater. Sci. Process 125 (6) (2019) 1–11.
[42] K.M. Rahulan, T. Sahoo, N.A. Little, I.P. Kokila, G. Vinitha, R.A. Sujatha, E ff ect of Sr 2 + doping on the linear and nonlinear optical properties of ZnO nanostructures, Opt Laser. Technol. 109 (2017) 313–318, 2019.
[43] Z. Sofiani, B. Sahraoui, M. Addou, R. Adhiri, M.A. Lamrani, L. Dghoughi, N. Fellahi, B. Derkowska, W. Bala, Third harmonic generation in undoped and X doped ZnO films (X: Ce, F, Er, Al, Sn) deposited by spray pyrolysis, J. Appl. Phys. 101 (6) (2007).
[44] J.T. Seo, S.M. Ma, Q. Yang, L. Creekmore, H. Brown, R. Battle, K. Lee, A. Jackson, T. Skyles, B. Tabibi, K.P. Yoo, Large optical nonlinearity of highly porous silica nanoaerogels in the nanosecond time domain, J. Kor. Phys. Soc. 48 (6) (2006) 1395–1399.
[45] H.S. Sindhu, S.R. Maidur, P.S. Patil, R.J. Choudhary, B.V. Rajendra, Tuning optical, electrical and magnetic properties of fiber structured ZnO film by deposition temperature and precursor concentration, Mater. Sci. Semicond. Process. 68 (2017) 97–107.
[46] P.P. Jeeju, S. Jayalekshmi, K. Chandrasekharan, P. Sudheesh, Enhanced linear and nonlinear optical properties of thermally stable ZnO/poly(styrene)-poly(methyl methacrylate) nanocomposite films, Thin Solid Films 531 (2013) 378–384.